Molecular dynamics studies of strongly coupled charged particle bilayers at finite temperatures

Z. Donkó
Research Institute for Solid State Physics and Optics of the Hungarian Academy of Sciences P.O. Box 49, H-1525 Budapest, Hungary

G. J. Kalman
Department of Physics, Boston College, Chestnut Hill, Massachusetts 02467

(Received 18 December 2000; published 23 May 2001)

The structure of strongly coupled charged particle bilayers was investigated using molecular dynamics simulation, in a wide range of the plasma coupling parameter $\Gamma = 20-100$. The simulations showed the existence of a series of structural transformations, controlled by the separation of the layers. At high values of Γ a pronounced long-range order was found to develop at intermediate layer separations, with staggered square lattice configuration. The results show a fair agreement with those obtained by hypernetted chain calculations, in terms of intralayer and interlayer pair correlation functions and structure functions.

DOI: 10.1103/PhysRevE.63.061504 PACS number(s): 64.70.Ja, 52.65.−y, 52.27.Gr

I. INTRODUCTION

Multilayered structures of charged particles can be realized in various physical systems, e.g., ion traps [1,2], semiconductor devices [3–6], and electrical discharges containing dust particles [7–10]. Bilayers, where the charged particles are confined in two quasi-two-dimensional layers represent the simplest form of multilayered systems. It was shown both experimentally [1] and theoretically [11–15] that bilayer systems exhibit different structural transformations when the system parameters are changed. In this study we consider only *symmetric* bilayers where the density of the (singly charged) particles is the same in both layers.

Bilayers consisting of *classical* point charges, which interact through the three-dimensional Coulomb potential can be characterized by two variables.

(i) The coupling parameter Γ defined in the same manner as in the case of a single layer (two-dimensional one-component plasma [16,17]):

$$\Gamma = \frac{q^2}{akT}, \tag{1}$$

where $a = (n\pi)^{-1/2}$ is the Wigner-Seitz (WS) radius (n is the surface density of particles, k is the Boltzmann constant, q is the charge of the particles, and T is the temperature).

(ii) The separation of the two layers, in units of the WS radius d/a.

Calculating the energies of different crystalline phases at *zero temperature*, Goldoni and Peeters identified a sequence of structural changes with changing the layer separation [18]. They have found that at very low layer separations a simple hexagonal phase has the lowest energy. With increasing layer separation the lattice is deformed to a staggered rectangular configuration, which subsequently changes to staggered square lattice, at approximately $d/a = 0.46$. The staggered square phase with further increasing layer separation (at $d/a = 1.1$) changes to staggered rhombic configuration and finally to staggered hexagonal form (at $d/a = 1.3$). The different lattice structures and the corresponding d/a values are shown in Fig. 1.

The first calculations for the static behavior of charged particle bilayers at nonzero temperatures were carried out by Valtchinov *et al.* [11,12] and Kalman *et al.* [13–15], using the hypernetted chain (HNC) technique [19]. This work has provided results for the liquid phase in terms of a catalogue of intralayer $g_{11}(r)$ and interlayer $g_{12}(r)$ pair correlation functions and the companion $S_{11}(k)$ and $S_{12}(k)$ structure functions, for a wide range of Γ and d/a values. The work also has shown that in the strongly coupled liquid phase a series of structural phase changes exist, not dissimilar to those found for the solid phase in Ref. [18].

In the analysis of the structures of two-dimensional (2D)

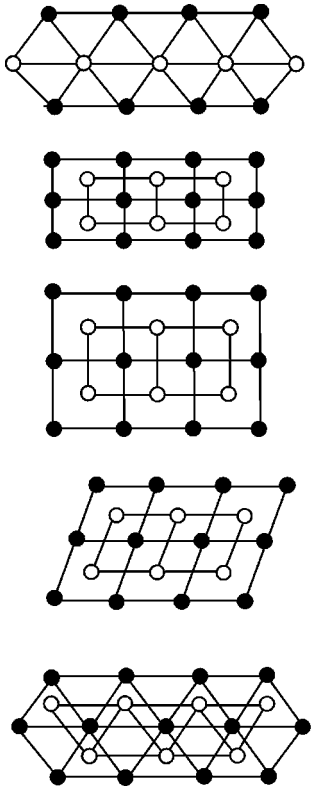

FIG. 1. The principal lattice configurations of symmetric bilayers at zero temperature, according to Ref. [18].

 ©2001 The American Physical Society

and 3D one component plasma (OCP) systems Monte Carlo (MC) and molecular dynamics (MD) studies have proven to be important complements to theoretical investigations [20–23]. With respect to the pair correlation function, the HNC calculations usually show wider and lower-amplitude peaks than the results of the MC or MD simulations. The study of charged particle bilayers via computer simulations also should provide important further insight into the static properties, correlation functions, etc., and, indirectly, into the phase structure of these systems.

Strongly coupled classical charged particle bilayers were generated by the NIST group [1,2] in cryogenic ion traps. The coupling parameter Γ in these experiments was high enough to bring the system in the crystalline phase. The various predicted layered structures [11,18] were observed at layer separations, which were in good agreement with theoretical values. Presently there are no experimental data on the strongly coupled liquid state, although such experimental data may become available in the near future. As to electronic bilayers, the r_s values for which 2D or layered semiconductor structures so far have been fabricated ($r_s<15$) are not high enough for structural transformations to be observed [5,24,25].

In this paper we report a molecular dynamics study of strongly coupled ($\Gamma \gg 1$) charged particle bilayers. Section II of the paper describes the simulation technique, while the results are presented in Sec. III. The summary of the work is given in Sec. IV.

II. SIMULATION TECHNIQUE

In the calculations the particle-particle particle-mesh (PPPM) method, developed by Hockney and Eastwood [26,27] was used. This method makes it possible to simulate large ensembles of particles interacting through long-range forces. The force of interaction in not truncated but it is partitioned to a long-range force (that can be represented on a mesh) and a short-range ''correction'' force—which, together with the mesh-force gives the exact (Coulomb) interaction force. We used a two-dimensional variant of the algorithm and transformed the two layers into a single layer where pairs of particles had interaction potentials according to

$$\begin{bmatrix} \phi_{11}\phi_{12} \\ \phi_{21}\phi_{22} \end{bmatrix} = q^2 \begin{bmatrix} r^{-1} & (r^2+d^2)^{-1/2} \\ (r^2+d^2)^{-1/2} & r^{-1} \end{bmatrix}, \qquad (2)$$

where ϕ_{ij} is the potential between two particles situated originally in layer i and j, respectively.

In the simulations presented here the number of particles was set to 1600 in both layers (with periodic boundary conditions) and at the start of the simulations random initial particle configurations were set up. The initial velocities of the particles were sampled from a Maxwellian distribution with a temperature corresponding to the prescribed value of Γ. The system was then thermostated for 6000 time steps, and the pair correlation functions were obtained in the next several thousand (2000–10 000) time steps following the thermostation period. The stability of the system was monitored by recording the temperature (calculated from the kinetic energy of particles). No observable self-heating occurred during the time of simulations. Tests of the simulation program in the limits of large and zero layer separations showed that the pair correlation functions are in very good agreement with those obtained from Monte Carlo simulations of a single two-dimensional layer of charged particles [21]. The effect of different initial configurations of particles was also tested and the sensitivity of the results on the initial conditions was found to be marginal.

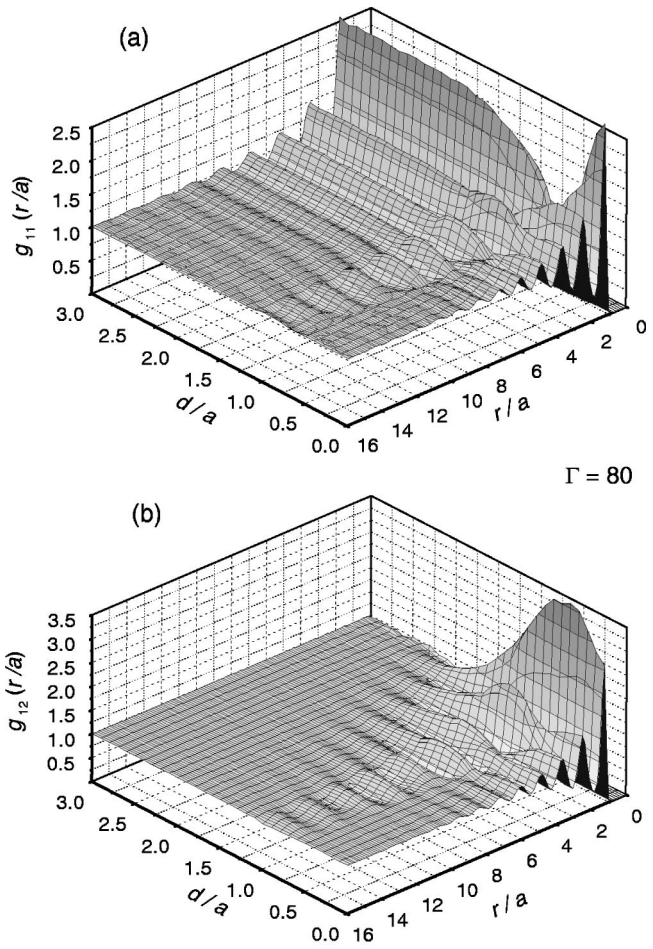

FIG. 2. Intralayer (a) and interlayer (b) pair correlation functions at $\Gamma=80$, obtained from the MD simulations.

The present calculations were carried out for $\Gamma=20$, 40, 60, 80, and 100 and for layer separations in the range $0 \leqslant d/a \leqslant 3$. The main results of the simulations are the intralayer $[g_{11}(r/a)]$ and interlayer $[g_{12}(r/a)]$ pair correlation functions. We also obtained snapshots of particle positions to illustrate the different structures arising, and determined the coordination numbers to investigate the changes between the different structural phases. The intralayer (ρ) and interlayer (σ) coordination numbers were calculated from the pair correlation functions

$$\rho_i = 2\pi n \int_{m_i}^{M_i} r g_{11}(r)\, dr, \qquad (3)$$

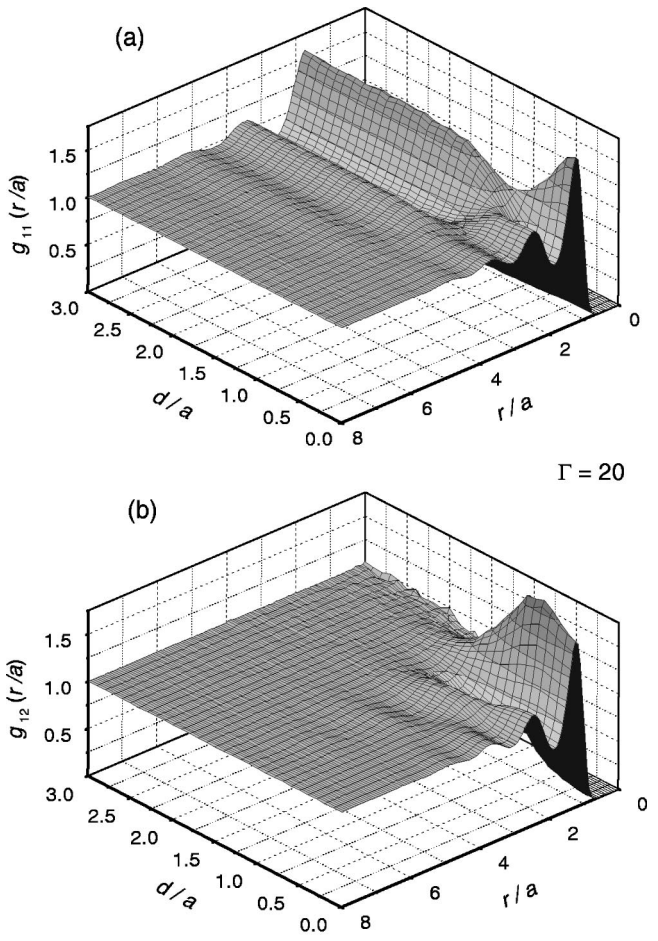

FIG. 3. Intralayer (a) and interlayer (b) pair correlation functions at $\Gamma=20$, obtained from the MD simulations.

$$\sigma_i = 2\pi n \int_{m_i}^{M_i} r g_{12}(r) dr, \tag{4}$$

where m_i and M_i are the positions of the minima of $g(r)$ preceding and following the ith peak of $g(r)$, respectively [11].

The bilayer system is also characterized by the intralayer and interlayer structure functions, which are calculated through the Hankel transform of the pair correlation functions:

$$S_{11}(k) = 1 + 2\pi n \int_0^{\infty} [g_{11}(r) - 1] r J_0(kr) dr, \tag{5}$$

$$S_{12}(k) = 2\pi n \int_0^{\infty} [g_{12}(r) - 1] r J_0(kr) dr, \tag{6}$$

where J_0 is the zero-th order Bessel function. In our calculations the integration was carried out up to a cutoff value of r (see later).

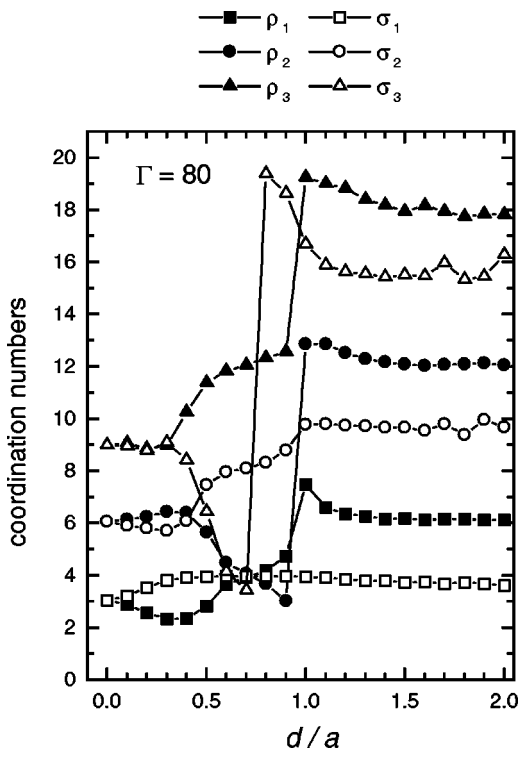

FIG. 4. The first three intralayer (ρ_1,ρ_2,ρ_3) and interlayer $(\sigma_1,\sigma_2,\sigma_3)$ coordination numbers as a function of d/a, for $\Gamma=80$.

III. RESULTS

The pair correlation functions obtained from the MD simulations at $\Gamma = 80$ are shown in Fig. 2. The plot of g_{12} [see Fig. 2(b)] indicates that at separations exceeding $d/a \approx 2.0$ there is no appreciable correlation between the two layers. Above this value of d/a the intralayer correlation function [see Fig. 2(a)] is the same as that of an isolated two-dimensional layer. As the layer separation is decreased, it is first the interlayer correlation function that shows the onset of coupling between the two layers. The intralayer correlation, however, remains practically unperturbed until $d/a \approx 1.4$ is reached. A remarkable feature of the system is the appearance of a pronounced long-range order at intermediate layer separation, around $d/a=0.8$, shown by both of the g_{11} and g_{12} functions. Here the order extends far beyond that in an isolated layer, indicating that at these intermediate values of d/a the two layers support each other to establish a long-range order. In this range of layer separation the system is in the staggered square configuration. The present finding is in agreement with recent observations of Schweigert *et al.* [28,29] who have found that among the different Wigner crystal configurations the square lattice has the highest melting temperature.

This enhanced long-range order, however, only develops at high values of Γ. At lower values, e.g., at $\Gamma=20$, no such effect is observed as it can be seen in Fig. 3, where the correlation functions are displayed. Nevertheless, the interlayer correlation is the strongest around $d/a \approx 0.6$.

The first three intralayer (ρ_1,ρ_2,ρ_3) and interlayer $(\sigma_1,\sigma_2,\sigma_3)$ coordination numbers calculated from the pair cor-

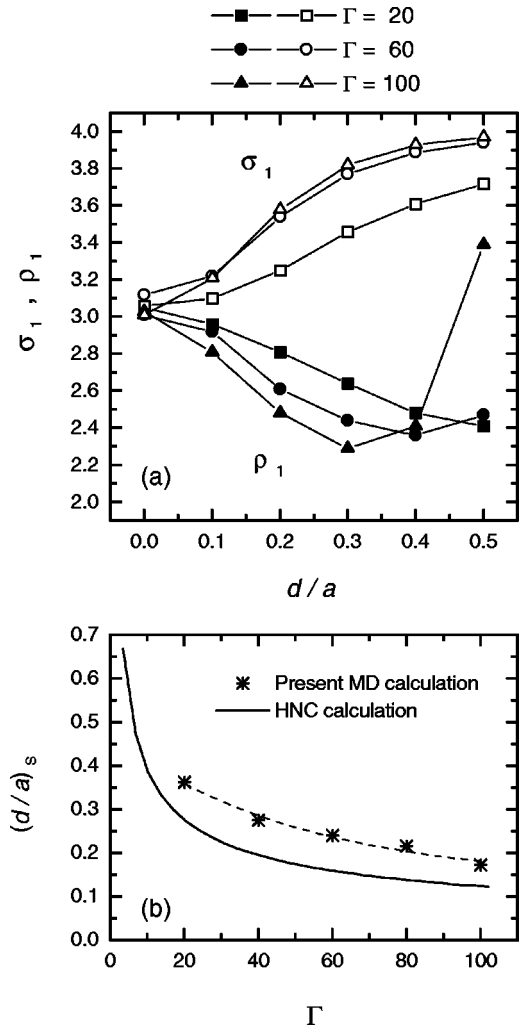

FIG. 5. (a) The dependence of the first shell coordination numbers ρ_1 and σ_1 on d/a, for different values of the coupling parameter Γ. (b) The limiting value of d/a, for which the substitutional disorder is dominant, as a function of Γ.

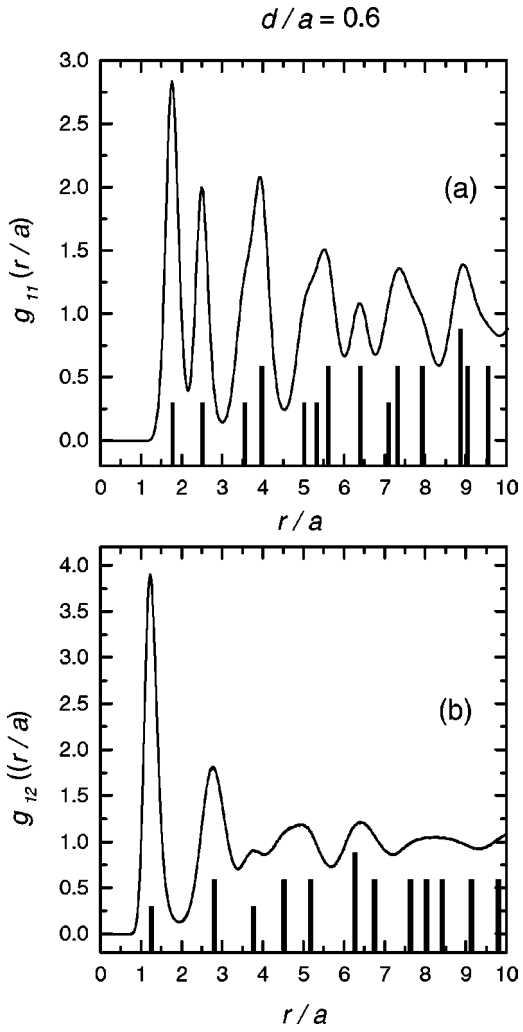

FIG. 6. Intralayer (a) and interlayer (b) pair correlation functions for $\Gamma=80$ and $d/a=0.6$. The heavy vertical lines indicate the positions of coordination shells for a perfect staggered square lattice; the height is proportional to the number of particles in the given shell.

relation functions [using Eqs. (3) and (4)] are plotted in Fig. 4, for $\Gamma=80$. At $d/a=0$, i.e., in the hexagonal phase, the coordination numbers ρ_1 and σ_1 are approximately equal to 3. This shows the existence of the substitutional disorder, where some of the particles occupy the sites appropriate for the other layer. The existence of this substitutional disorder was already found by the HNC calculations [11,14]. In the absence of disorder $\rho_1=2$ and $\sigma_1=4$ should hold, which values are actually approached with increasing d/a.

With increasing layer separation the coordination numbers clearly show the formation of the staggered square lattice configuration, in the $0.6\leqslant d/a\leqslant 0.8$ range. This structure is characterized by $\rho_1=\rho_2=\sigma_1=\sigma_3=4$, and $\sigma_2=8$. The value $\rho_3=12$ shows that two closely separated shells situated at $r/a=3.545$ and $r/a=3.963$ are not resolved in $g_{11}(r/a)$ due to the nonperfect lattice structure. It is noted that according to the calculations of Goldoni and Peeters [18] the staggered square configuration has the lowest energy at layer separations $0.46<d/a<1.1$. In our case this structure is established at somewhat higher values of d/a, compared to the zero-temperature, perfect-lattice calculations. We have verified, however, that the onset of this structure is shifted towards lower d/a values when Γ is increased.

As the layer separation is further increased, around $d/a=0.9$, a sudden change of the coordination numbers is observed (see Fig. 4). On the other hand, according to Ref. [18] the staggered square phase is transformed continuously to staggered hexagonal structure through a rhombic form. The abrupt change in the coordination numbers is caused by the fact that the coordination shells that would be narrowly separated by less than a critical distance in the solid phase are not resolved in the liquid phase. Thus a small change in the underlying lattice structure may cause a sudden merging of two adjacent shells and result in a correspondingly enlarged coordination number. The coordination numbers at layer separations above $d/a\approx 1.3$, $\rho_1=6$, $\rho_2=12$, and $\rho_3=18$ correspond to the hexagonal lattice structure, found within both layers.

The dependence of the substitutional disorder on Γ is in-

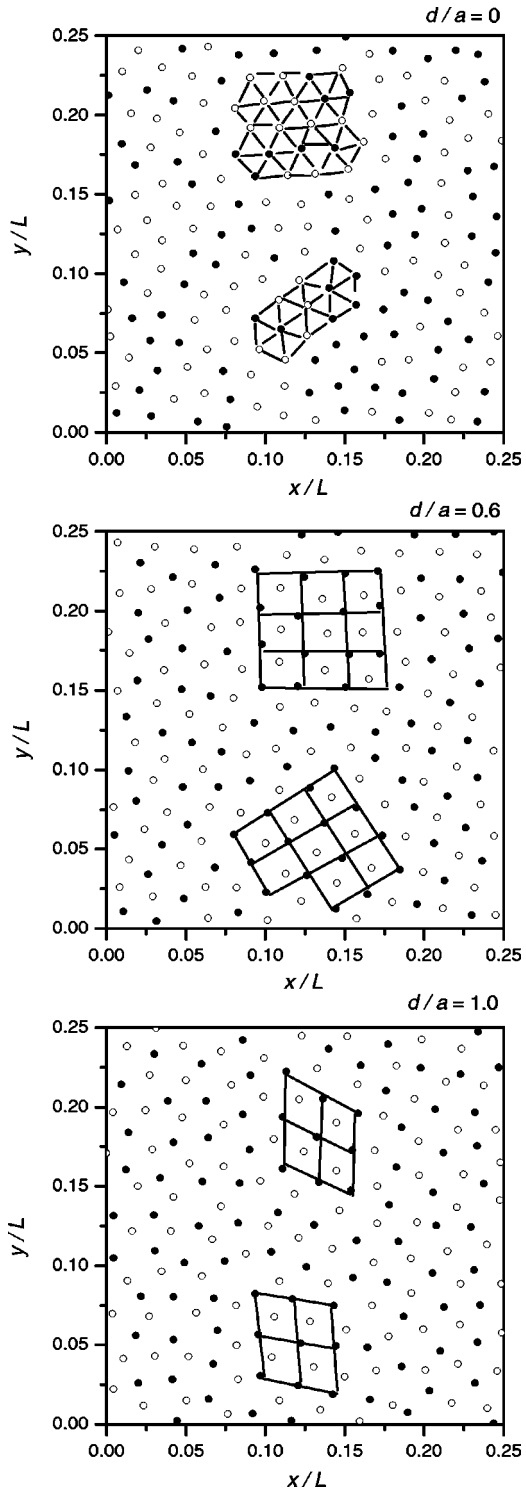

FIG. 7. Snapshots of particle positions at different layer separations at $\Gamma=80$. The figures show superimposed view of the two layers; they display one quarter of the $L_s\times L_s$ simulation square. (a) $d/a=0$, (b) $d/a=0.6$, (c) $d/a=1.0$. The particles situated in layers 1 and 2 are represented by filled and open circles, respectively.

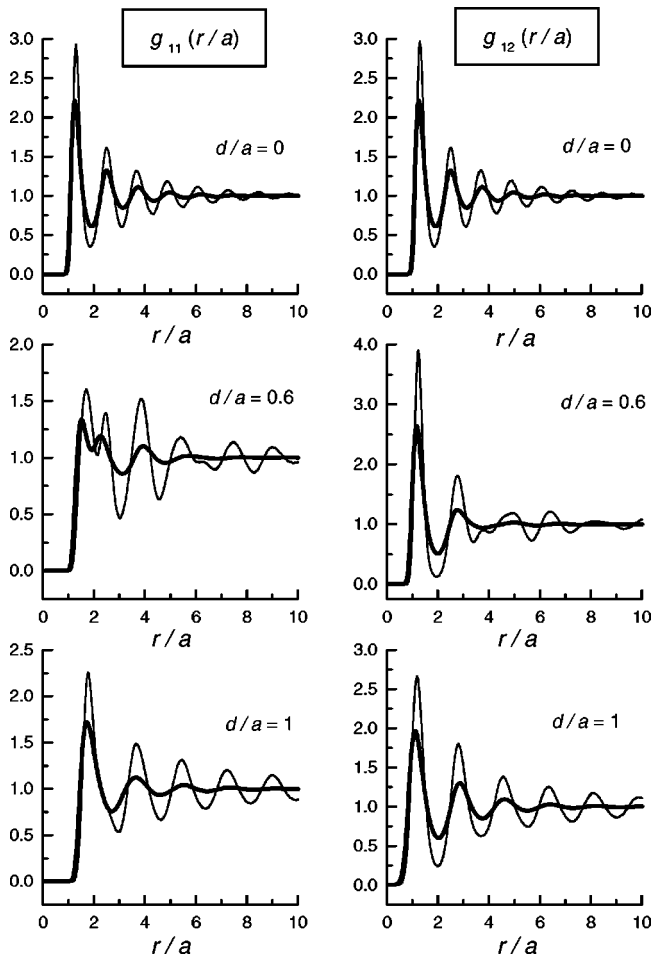

FIG. 8. Intralayer (g_{11}) and interlayer (g_{12}) pair correlation functions obtained from MD (thin line) and HNC (heavy line) calculations, for different layer separations, at $\Gamma=80$.

vestigated in Fig. 5. Figure 5(a) shows the coordination numbers ρ_1 and σ_1 as a function of d/a, for different values of Γ. The substitutional disorder disappears faster at higher Γ. We can say that the disorder is dominant as long as $\sigma_1-\rho_1<1$ (at $d/a=0$, i.e. in the case of complete disorder $\sigma_1-\rho_1=0$, while in the ordered hexagonal phase, in the absence of disorder $\sigma_1-\rho_1=2$). Figure 5(b) shows the value of the layer separation $(d/a)_S$ as a function of Γ where the ''disorder parameter,'' $\sigma_1-\rho_1$ reaches 1. The layer separations obtained this way are in fair agreement with those obtained from the theoretical calculations yielding $(d/a)_S=1.23\Gamma^{-1/2}$ [11] [see Fig. 5(b)].

The present MD simulations give very accurately the positions of the peaks of the pair correlation functions. This is illustrated in Fig. 6, where $g_{11}(r/a)$ and $g_{12}(r/a)$ are plotted for $\Gamma=80$ and $d/a=0.6$, together with the peak positions corresponding to a perfect staggered square lattice.

Snapshots of particle positions obtained at $\Gamma=80$ and $d/a=0$, 0.6, and 1.0 are displayed Fig. 7. At $d/a=0$ the hexagonal structure clearly appears in some regions (recall that at $d/a=0$, $\Gamma=80\sqrt{2}\approx 112$, which still belongs to the fluid phase of a single isolated layer). The staggered square structure is pronounced at $d/a=0.6$, while at the highest layer separation $d/a=1$, the staggered square configuration is basically wiped out and some grains with staggered rhombic structure can be identified [see Fig. 7(c)]. In our case the staggered hexagonal structure, predicted at $T=0$ for large

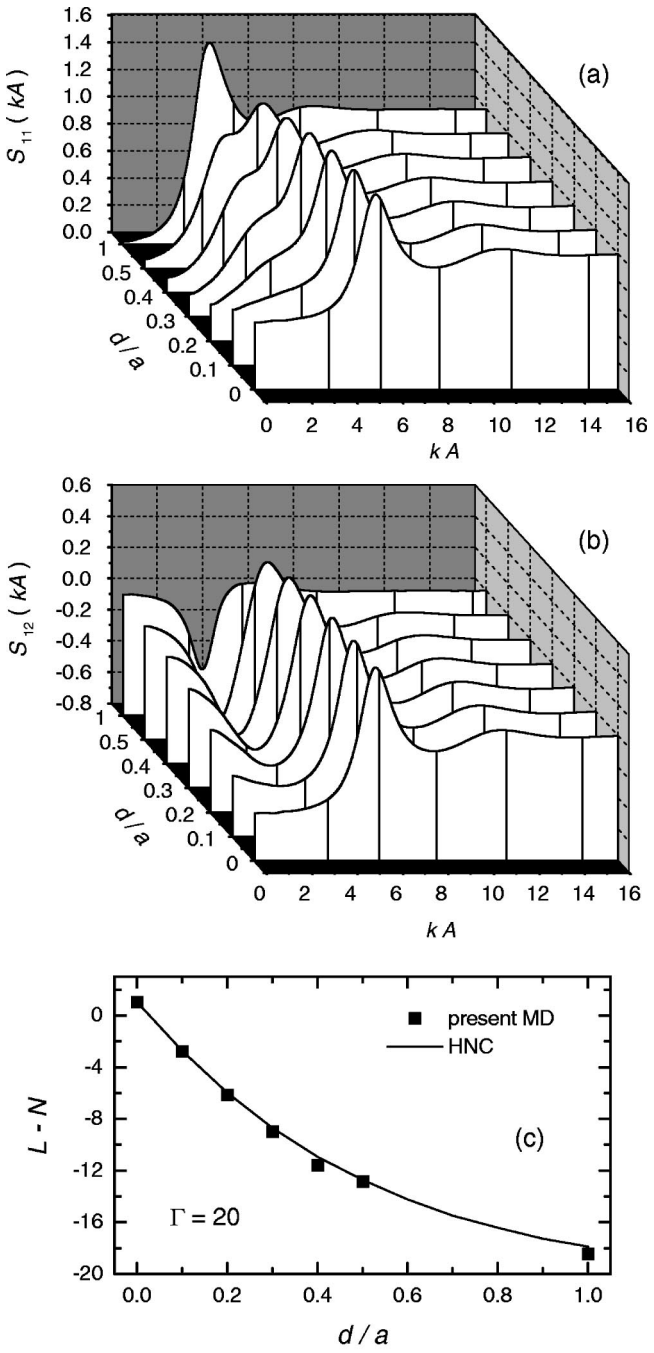

FIG. 9. (a),(b) Structure functions of the charged particle bilayer for selected values of d/a, at $\Gamma=20$. (c) Difference of diagonal (L) and off-diagonal (N) elements of the inverse compressibility matrix as a function of d/a, extracted from $S(k)$ data ($\Gamma=20$).

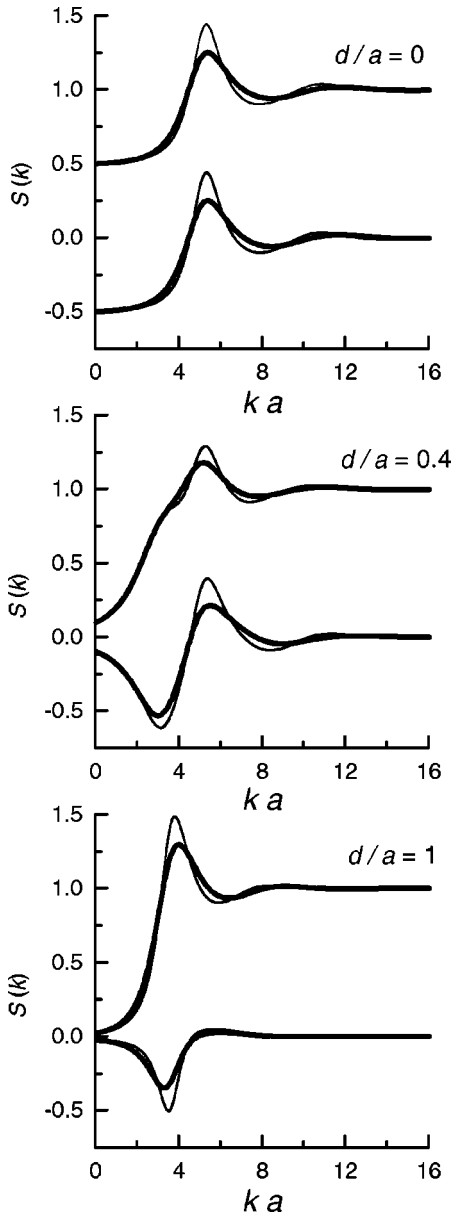

FIG. 10. Intralayer $S_{11}(k)$ and interlayer $S_{12}(k)$ structure functions obtained from MD (thin line) and NHC (heavy line) calculations, for different layer separations, at $\Gamma=20$.

layer separations, cannot be observed by looking at particle positions, due to the kinetic energy of the particles which dominates over the interlayer potential energy in this range of d/a.

The pair correlation functions obtained from the present MD simulations are compared to those of the HNC calculations in Fig. 8, for $\Gamma=80$. When the two layers are not separated, the positions of the peaks of the HNC pair correlation functions are the same as in the case of MD data. The heights of the peaks are, however, significantly ($\approx 25\%$) smaller in the case of HNC results. The MD data at the same time predict stronger long-range order. This is even more pronounced at intermediate layer separations, e.g., at $d/a=0.6$, as illustrated in Fig. 8(b). Here the HNC predicts a long-range order up to $r/a\approx 6$, while the pair correlation functions obtained from the MD simulations exhibit peaks well beyond this limit. In this case even the positions of the peaks show a small difference, indicating that the two techniques predict somewhat different structures.

The $S_{11}(k)$ and $S_{12}(k)$ structure functions obtained from the MD calculations are plotted in Figs. 9(a) and 9(b) for selected values of the layer separation d/a, at $\Gamma=20$. The values of the structure functions taken at $k=0$ satisfy the perfect screening sum rule within the uncertainty of the cal-

culations (see, e.g., Ref. [11]):

$$S_{11}(k=0) = -S_{12}(k=0) = S_0 . \quad (7)$$

The relation between S_0 and the diagonal (L) and off-diagonal (N) elements of the inverse compressibility matrix [14]

$$S_0 = \frac{1}{2} \frac{1}{L-N+2(d/a)\Gamma} \quad (8)$$

also makes it possible to obtain $L-N$ as a function of the layer separation. The results obtained from the MD data, as well as the results of the HNC calculations are displayed in Fig. 9(c), for $\Gamma = 20$. Good agreement is found between the two sets of data obtained by the different techniques.

The $S_{11}(k)$ and $S_{12}(k)$ structure functions obtained from the MD and HNC calculations are compared in Fig. 10, where the data are presented for $\Gamma = 20$. The agreement between the two sets of data is acceptable, the MD simulations result $S(k)$ functions with higher and sharper peaks compared to the HNC calculations, in accordance with the differences in pair correlation functions.

Based on the present MD simulations, the structure functions could be determined only for the $\Gamma \leqslant 40$ range of the coupling parameter. We have encountered difficulties when we tried to calculate the structure functions at higher values of Γ, where the long-range order extends to very high r/a values. At $\Gamma = 80$, in the staggered square phase the long-range order has been observed even at the limiting r/a value $[(r/a)_{\max} = 17.7]$ in our simulations. In order to obtain the structure functions at these high values of Γ with a good accuracy, the size of the system (number of particles) should significantly be increased. Even in the $\Gamma \leqslant 40$ range the cutoff value of r/a used in the evaluation of structure functions [Eqs. (5) and (6)] had to be chosen carefully, to avoid the influence of the statistical noise of the $g(r/a)$ functions at high values of r/a. [The structure functions presented here were calculated using $(r/a)_{\text{cutoff}} = 7.3$.]

IV. SUMMARY

In this paper, we have reported the results of molecular dynamics simulations of strongly coupled, classical, symmetric charged particle bilayers. The simulations show a sequence of structural changes as the separation of the two layers is increased. We also observe a substitutional disorder at low layer separations and its gradual disappearance with increasing d/a. Our calculations show that at higher Γ values (e.g., $\Gamma = 80$) and at intermediate layer separations a very pronounced long-range order, with staggered square particle positions develops at intermediate layer separations $0.6 \leqslant d/a \leqslant 0.8$. This observation is in agreement with recent theoretical findings that the staggered square phase of the bilayer Wigner crystal is the most stable amongst the possible lattice configurations.

The intralayer and interlayer pair correlation functions, as well as the structure functions are found to be in fair agreement with those obtained in previous hypernetted chain (HNC) calculations. The MD data show that a more pronounced structure is established within and between the layers, compared to the predictions of the HNC method. The structure functions obtained from our simulations are found to satisfy the perfect screening sum rule $S_{11}(k=0) = -S_{12}(k=0) = S_0$. The dependence of S_0 and that of the difference of the diagonal and off-diagonal elements of the inverse compressibility matrix $(L-N)$ on d/a show a good agreement with the results of HNC calculations. The statistical noise of the molecular dynamics simulation and the limited range of particle separations (r/a) for which the pair correlation functions could be determined, have restricted the range of Γ for which the $S(k)$ functions could be calculated.

ACKNOWLEDGMENTS

This work was partly supported by Grants DE-FG02-98ER54501, INT-0002200 (G.J.K.), OTKA-T-25989, OTKA-T-34156, MTA-OTKA-NSF-28, and a Bolyai Grant from the Hungarian Academy of Sciences (Z.D.). We thank G. McMullan for providing additional HNC data.

[1] T.B. Mitchell, J.J. Bollinger, D.H.E. Dubin, X.-P. Huang, W.M. Itano, and R.H. Bundham, Science **282**, 1290 (1998).

[2] J.J. Bollinger, T.B. Mitchell, X.-P. Huang, W.M. Itano, J.N. Tan, B.M. Jelenković, and D.J. Wineland, Phys. Plasmas **7**, 7 (2000).

[3] J. Jo, Y.W. Suen, L.W. Engel, M.B. Santos, and M. Shayegan, Phys. Rev. B **46**, 9776 (1992).

[4] F. Rapisada and G. Senatore, in *Strongly Coupled Coulomb Systems*, edited by G. Kalman, K. Blagoev, and M. Rommel (Plenum, New York, 1998).

[5] I.S. Millard, N.K. Patel, M.Y. Simmons, E.H. Linfield, D.A. Ritchie, G.A.C. Jones, and M. Pepper, Appl. Phys. Lett. **68**, 3323 (1996).

[6] C.B. Hanna, D. Haas, and J.C. Diaz-Velez, Phys. Rev. B **61**, 13 882 (2000).

[7] A. Melzer, V.A. Schweigert, I.V. Schweigert, A. Homann, S. Peters, and A. Piel, Phys. Rev. E **54**, R46 (1996).

[8] J.B. Pieper, J. Goree, and R.A. Quinn, J. Vac. Sci. Technol. A **14**, 519 (1996).

[9] S. Nunomura, D. Samsonov, and J. Goree, Phys. Rev. Lett. **84**, 5141 (2000).

[10] M. Rosenberg, J. Phys. IV **10**, Pr5-73 (2000).

[11] V.I. Valtchinov, G. Kalman, and K.B. Blagoev, Phys. Rev. E **56**, 4351 (1997).

[12] V. Valtchinov, G.J. Kalman, and K.I. Golden, in *Strongly Coupled Coulomb Systems*, edited by G. Kalman, K.B. Blagoev and M. Rommel (Plenum Press, New York, 1998), p. 533.

[13] G. Kalman, V. Valtchinov, and K.I. Golden, in *Condensed Matter Theories*, edited by J. Providencia and F.B. Malik (Nova Science Publishers, Commack, NY, 1998), Vol. 13, p. 209.

[14] G.J. Kalman, K.B. Blagoev, Z. Donkó, K.I. Golden, G. McMullan, V. Valtchinov, and H. Zhao, J. Phys. IV **10**,

Pr5-85 (2000).
[15] G.J. Kalman, Z. Donkó, K.I. Golden, and G. McMullan (unpublished).
[16] M. Baus and J.-P. Hansen, Phys. Rep. **59**, 1 (1980).
[17] S. Ichimaru, Rev. Mod. Phys. **54**, 1017 (1982).
[18] G. Goldoni and F.M. Peeters, Phys. Rev. B **53**, 4591 (1996).
[19] F. Lado, Phys. Rev. B **17**, 2827 (1978).
[20] H. Totsuji, Phys. Rev. A **17**, 399 (1978).
[21] R.C. Gann, S. Chakravarty, and G.V. Chester, Phys. Rev. B **20**, 326 (1979).
[22] W.L. Slattery, G.D. Doolen, and H.E. DeWitt, Phys. Rev. A **26**, 2255 (1982).
[23] G. Zwicknagel, D. Klakow, and P.-G. Reinhard, Contrib. Plasma Phys. **33**, 395 (1993).
[24] S. Shapira, U. Sivan, P.M. Solomon, E. Buchstab, M. Tischler, and G. Ben Yoseph, Phys. Rev. Lett. **77**, 3181 (1996).
[25] S. Shapira, E.H. Linfield, and M. Pepper, Appl. Phys. Lett. **74**, 1603 (1999).
[26] R.W. Hockhey and J.W. Eastwood, Comput. Phys. Commun. **19**, 215 (1980).
[27] R.W. Hockhey and J.W. Eastwood, *Computer Simulation Using Particles* (McGraw-Hill, New York, 1981).
[28] I.V. Schweigert, V.A. Schweigert, and F.M. Peeters, Phys. Rev. Lett. **82**, 5293 (1999).
[29] I.V. Schweigert, V.A. Schweigert, and F.M. Peeters, J. Phys. IV **10**, Pr5-117 (2000).